ESRF	**Experiment title:** Chemical order and crystal phase transition in small magnetic FeRh nanoparticles	**Experiment number**: 32-03-745
Beamline: BM32	**Date of experiment**: from: 10/11/2020 to: 19/11/2020	**Date of report**: 30/08/2021
Shifts: 18	**Local contact(s)**: Lucio Martinelli & Gilles Renaud	*Received at ESRF:*

Names and affiliations of applicants (* indicates experimentalists):

*Dr. Ingrid Cañero Infante, *Institut des Nanotechnologies de Lyon, UMR5270 CNRS ECL INSA UCBL CPE - Ecully*

*Dr. Florent Tournus, *Institut Lumière Matière, UMR5306, Université Lyon 1-CNRS, Université de Lyon - Villeurbanne*

Report:

Context and experimental conditions

The aim of the experiment was to investigate the chemical ordering of size-selected FeRh nanoparticles, from the A1 phase (fcc) to the B2 phase (CsCl-like). Several samples were studied, either embedded in amorphous carbon (on a Si substrate) or on perovskite substrates: $SrTiO_3$ (STO) single crystal or $BaTiO_3$ (BTO) thin films grown on STO. Different incident particle sizes have been considered, around 3.3 nm (corresponding to a 300 V deviation potential in the MSLECBD setup for nanoparticle deposition at ILM) and around 6.2 nm (corresponding to a 1200 V deviation potential). While random deposition of nanoparticles leads to powder-like patterns (rings in the surface plane of reciprocal lattice), it had been shown that on BTO the FeRh particles can adopt specific orientations after annealing (cf. report 32-03 734). These preferential orientations correspond to two different "cube on cube" epitaxy relationships. It should also be noted that the diffracted intensity is then higher once the particles have adopted coherent orientation with respect to the crystalline substrate. This is why in the previous experiments we were not able to detect FeRh in the A1 phase or randomly oriented particles in the B2 phase (diluted reference samples).

Measurements have been carried under UHV in the INS2 chamber, from room temperature up to 670°C. The x-ray energy was set to 15.8 keV. Scans have been performed in the surface plane (in various directions), with reciprocal space mapping for some samples, as well as a few scans in the direction perpendicular to the surface (L-scans) at specific locations. GISAXS patterns have also been acquired for selected samples, at different temperatures, to follow the particle size evolution.

Samples studied

In the present report, we show results on 4 different samples (labelled with their codename):

-**Sample TM2023**, made of 2 layers of FeRh particles (incident size of 6.2 nm), each one corresponding to an equivalent thickness of 10 Å (mean first-neighbor distance similar to the diameter, many multimers and the mean diameter is then around 8 nm), with a carbon over-layer and under-layer and a silicon substrate. This sample had been annealed at 700°C at ILM, before measurements at ESRF.

-**Sample TM2040**, made of 3 layers of FeRh particles (incident size of 6.2 nm), each one corresponding to an equivalent thickness of 5 Å (mean first-neighbor distance around 9 nm, many multimers and the mean diameter is then between 7 and 8 nm), with a carbon over-layer and under-layer and a silicon substrate. This sample was measured as-prepared and in-situ annealed at BM32 beamline.

-**Sample TM2030**, made of one layer of FeRh particles (incident size of 6.2 nm), corresponding to an equivalent thickness of 10 Å (mean first-neighbor distance similar to the diameter, many multimers and the mean diameter is then around 8 nm), deposited on a BTO thin film on STO single crystal, with a carbon layer capping. This sample was measured as-prepared and in-situ annealed (directly at 670°C) at BM32 beamline.

-**Sample TM2028**, made of one layer of FeRh particles (incident size of 3.3 nm), corresponding to an equivalent thickness of 5 Å (mean first-neighbor distance similar to the diameter, many multimers and the mean diameter is then around 4.1 nm), deposited on a STO single crystal, with a carbon layer capping. This sample was measured as-prepared and in-situ annealed (progressively) at BM32 beamline.

Main results

-**Sample TM2023**: peaks corresponding to the B2 phase of FeRh are clearly observed (see Fig. 1). From the peak width (FWHM), a crystal size around 7.8 nm diameter can be estimated, which is in agreement with the expected particle size.

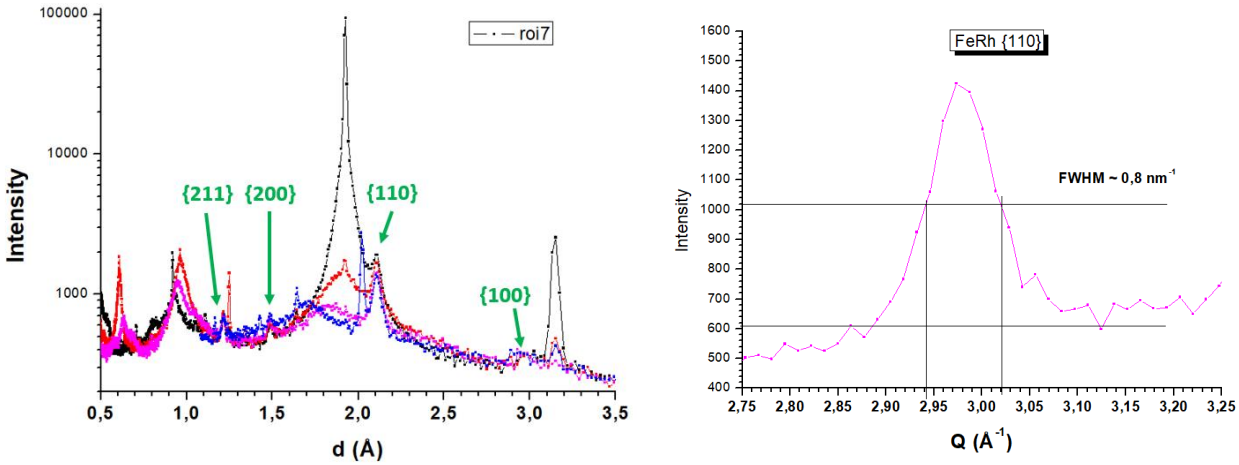

Fig. 1: x-ray diffracted intensity along different directions in the surface plane (left). The most intense peaks are due to the Si substrate, but FeRh B2 phase is clearly detected. Close view of the FeRh {110} peak (right) with a measure of its FWHM in order to estimate the crystal size.

-**Sample TM2040**: a broad peak corresponding to {111} (d ~2.16 Å) of the FeRh A1 phase is observed for the as-prepared sample. Upon annealing, this peak is shifted (towards d~2.13 Å) and become narrower. The corresponding estimated crystal size evolves from ~3 nm at room temperature (meaning that the crystal domain size of as-prepared particles is lower than the geometric size of particles) to ~7 nm at 670°C. Other peaks corresponding to the B2 phase of FeRh are also clearly observed (see Fig. 2), for temperature of 500°C and higher. Since the estimated diameter (from peak FWHM) is in line with the expected particle size, coalescence effects seems to be limited, the change in peak width should then reflect the crystallization taking place inside the particles.

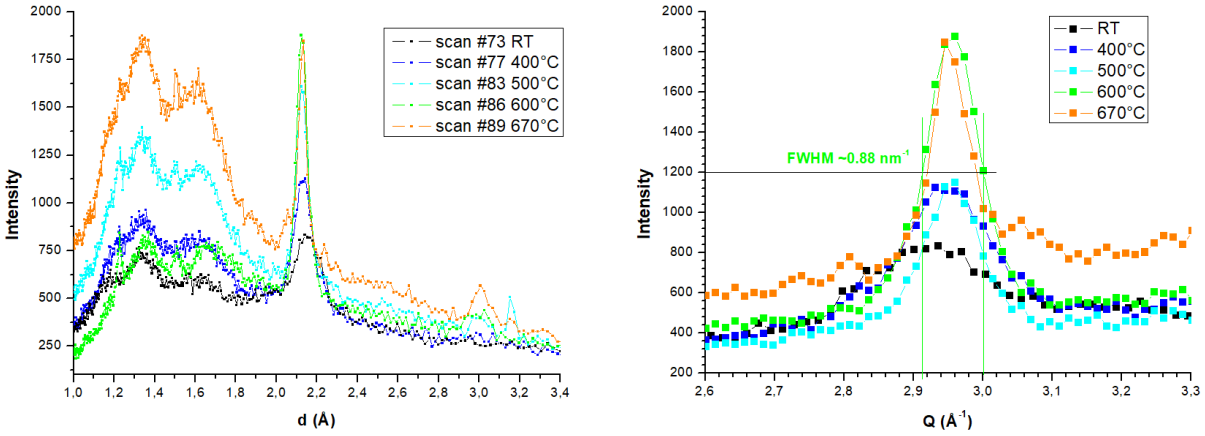

Fig. 2: x-ray diffracted intensity along different directions in the surface plane (left). Peaks corresponding to the FeRh B2 phase are detected ({100} at d~3.0 Å, {110} at d~2.1 Å, {200} at d~1.5 Å and {211} at d~1.2 Å). Close view of the FeRh {110} peak (right) with a measure of its FWHM in order to estimate the crystal size. The A1 to B2 phase transition is clearly visible, together with an increase in crystal size.

-**Sample TM2030**: a broad peak corresponding to {111} (d ~2.16 Å) of the FeRh A1 phase is observed for the as-prepared sample. Upon annealing (directly to 670°C), this peak is shifted (towards d~2.13 Å) and become narrower (see Fig. 3). The corresponding estimated crystal size evolves from ~3 nm at room temperature to ~18 nm at 670°C, which is the sign of consequent coalescence effect (even if we may still have particles with their initial size… the determination of the size distribution is hardly possible). This change of size is also visible from GISAXS measurements (see Fig. 4). The difference with respect with sample TM2023 (also with 10 Å cluster layer) where no such coalescence was observed, may be due to the presence of BTO surface or to a higher temperature annealing at BM32 compared to ILM lab (note however that for sample TM2040, with a 5 Å cluster layer but the same in-situ annealing procedure, no such coalescence was observed, cf. above). After annealing, the various peaks corresponding to the B2 phase of FeRh are also clearly observed, in particular the {100} peak which only exists in the case of a chemically ordered crystal.

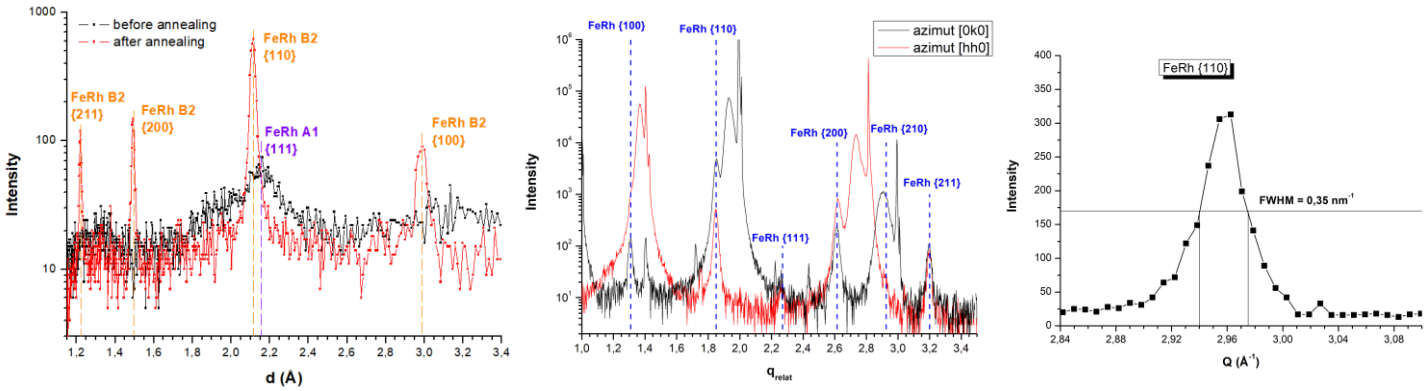

Fig. 3: Left: comparison of x-ray diffracted intensity (radial scan along an "intermediate" direction in the surface plane, avoiding the BTO/STO peaks) before and after annealing, measured at room temperature. Middle: x-ray diffracted intensity, at room temperature but after annealing, measured with radial scans in the surface plane along either [0k0] or [hh0] directions of the BTO lattice. Peaks corresponding to the FeRh B2 phase are clearly visible (here plotted as a function of q_{relat}, the wave vector normalized by the STO basis vector). Right: close view of the FeRh {110} peak with a measure of its FWHM in order to estimate the crystal size, after annealing.

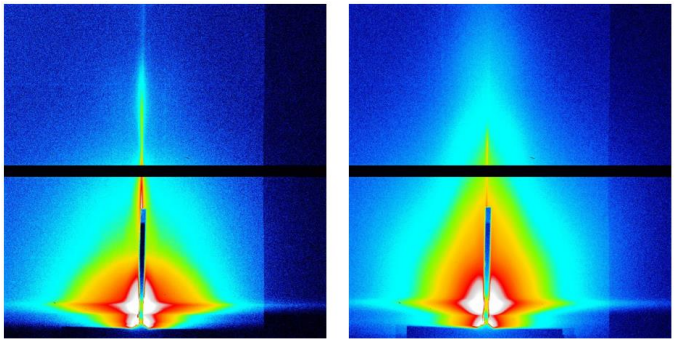

Fig. 4: GISAXS pattern measured for an as-prepared sample (TM2039, same initial particles), on the left, and after annealing, on the right. Qualitatively, annealing goes with a lateral size increase but also with a change in shape (surface wetting, particles are not spherical).

In addition to radial scans in given directions, a reciprocal space map of the surface plane has been measured (see Fig. 5). We clearly observe rings, of varying intensity, corresponding to FeRh B2 phase. This indicates that the sample is made of different "families" of particles: some with preferential orientations (already observed, cf. report 32-03 734) corresponding to the two "cube-on-cube" epitaxy relationships (cf. Fig. 5: $[100]_{FeRh}//[110]_{BTO}$ & $[001]_{FeRh}//[001]_{BTO}$, the usual epitaxy and an unusual one $[100]_{FeRh}//[100]_{BTO}$ & $[001]_{FeRh}//[001]_{BTO}$); and some particles with random orientations on the surface (note in particular that the appearance of a {111} peak of FeRh in the surface plane is not possible only with particles having their $[001]_{FeRh}$ direction perpendicular to the surface).

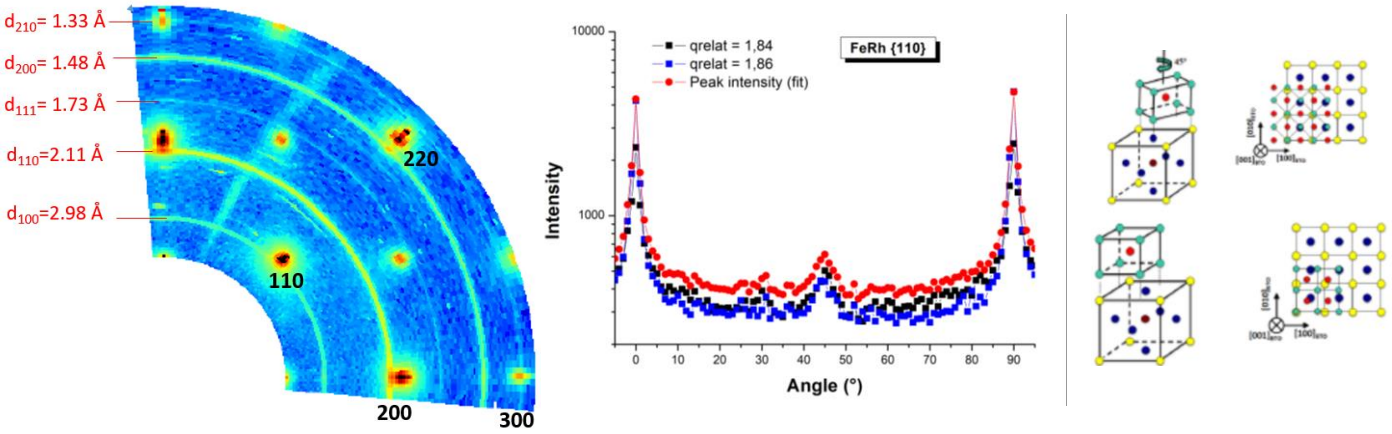

Fig. 5: Left: reciprocal space map in the surface plane. Spots corresponding to BTO and STO crystals are visible, together with rings corresponding to the FeRh B2 phase. These rings are not homogeneous as the diffracted intensity depends on the angle with the substrate lattice, showing higher intensity in particular preferential orientations: [h00] and [hh0] azimuths. Middle: diffracted intensity of the FeRh {110} peak as a function of the angle (0° corresponds to [h00] azimuth, while 45° corresponds to [hh0] azimuth. The background intensity has been subtracted, and the intensity determined with various procedures: the existence of two preferential orientations is visible. Right: illustration of the two "cube-on-cube" epitaxy relationships. The usual epitaxy ($[100]_{FeRh}//[110]_{BTO}$ & $[001]_{FeRh}//[001]_{BTO}$) corresponds to the major contribution.

-**Sample TM2028**: this sample is made of initially smaller particles (3.3 nm incident diameter) and has been studied with a progressive annealing. Before annealing, the FeRh {111} peak of the A1 phase is detected, with the same intensity along various azimuths, and the peak width indicates a crystal size around 2.5 nm. Starting from 500°C, peaks corresponding to the B2 phase are detected, and their intensity continue to increase with the temperature, while the FWHM become smaller (see Fig. 6). This shows that particle coalescence is concomitant with the B2 phase transition: from 500°C to 700°C the crystal size increase from about 10 nm to around 17 nm, a value significantly higher than the initial size of FeRh on the surface. This coalescence effect (also seen with GISAXS, see Fig. 7) is thus similar to the one observed for TM2030 and surprisingly leads to an identical final size even though the deposited particle diameter and surface density are smaller for TM2028. Once again, this may be due to a specific behavior of clusters on perovskite substrates.

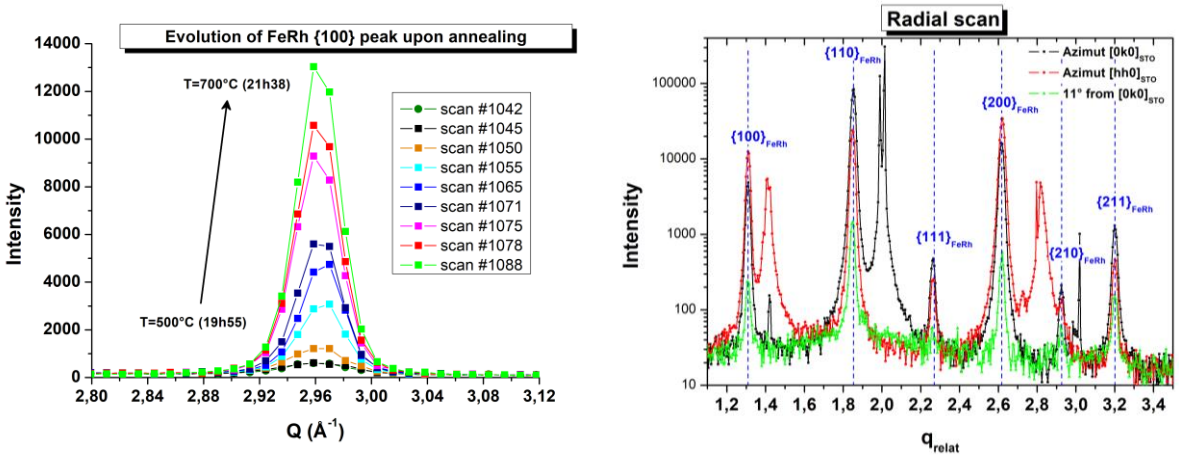

Fig. 6: Left: evolution of the {100} peak of FeRh in the B2 phase as a function of the annealing temperature, showing the increasing intensity concomitant with the peak narrowing. Right: radial scans (in the surface plane), after annealing, along different directions. Peaks corresponding to the B2 phase of FeRh are clearly seen and the intensity depends on the azimuth.

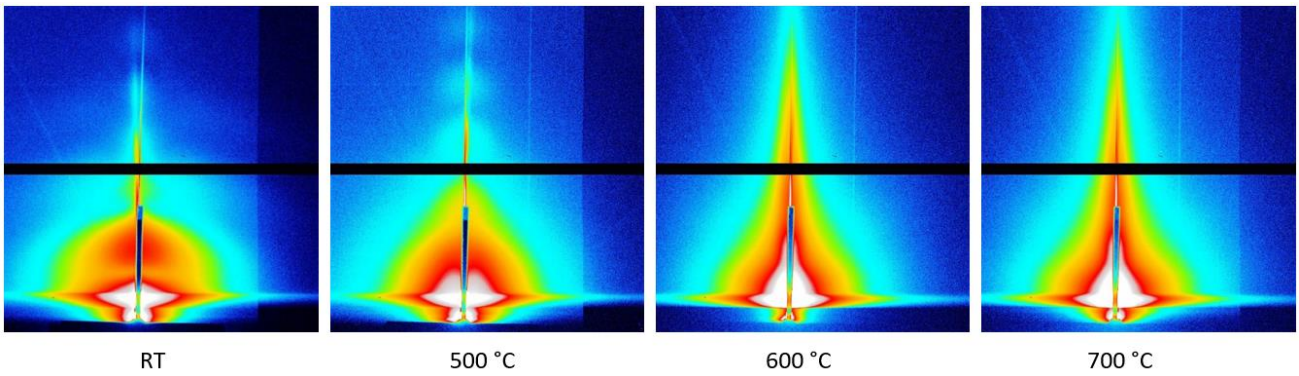

Fig. 7: GISAXS pattern measured for the as-prepared sample (at room temperature, on the left) and as a function of the annealing temperature. Qualitatively, annealing goes with a lateral size increase but also with a change in shape (surface wetting, particles are not spherical).

In addition to radial scans in given directions (see Fig. 6, right), a reciprocal space map of the surface plane has been measured after annealing (see Fig. 8). We clearly observe rings of varying intensity, corresponding to FeRh particles in the B2 phase with some orientations being more favorable. These observations can be accounted by considering different "families" of particles: some particles displaying as before (see above) the two "cube-on-cube" epitaxy relationships (see Fig. 8, left) and thus lying on a {001} facet; some other particles lying on a {110} facet and with a favorable coincidence between $\{211\}_{FeRh}$ and $\{310\}_{STO}$ (see Fig. 8, right); and finally some particles with random orientations on the surface. This explains the many peaks observed in the angular scans for different FeRh peaks (see Fig. 9). From the peak position and width, the different families of FeRh particles may correspond to slightly different cell parameters (different strain for the different epitaxy relationships) but the typical crystal size are apparently the same.

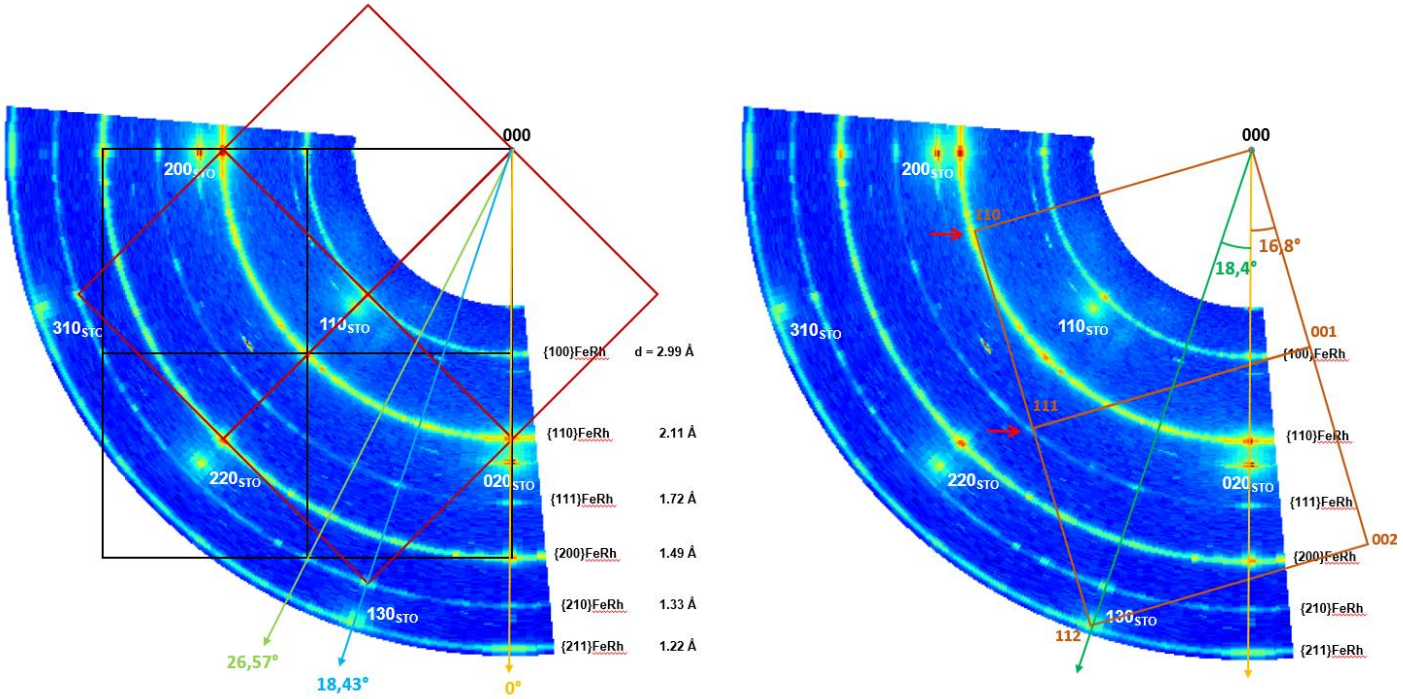

Fig. 8: reciprocal space map in the surface plane where STO peaks and rings corresponding to FeRh in the B2 are visible. On each ring, the intensity varies with the angle displaying peaks for some orientations corresponding either to FeRh particles on a {001} facet with the two "cube-on-cube" epitaxy relationships (left), or to FeRh particles on a {110} facet with a favorable coincidence between $\{211\}_{FeRh}$ and $\{310\}_{STO}$ (right, with one particular coincidence schematized).

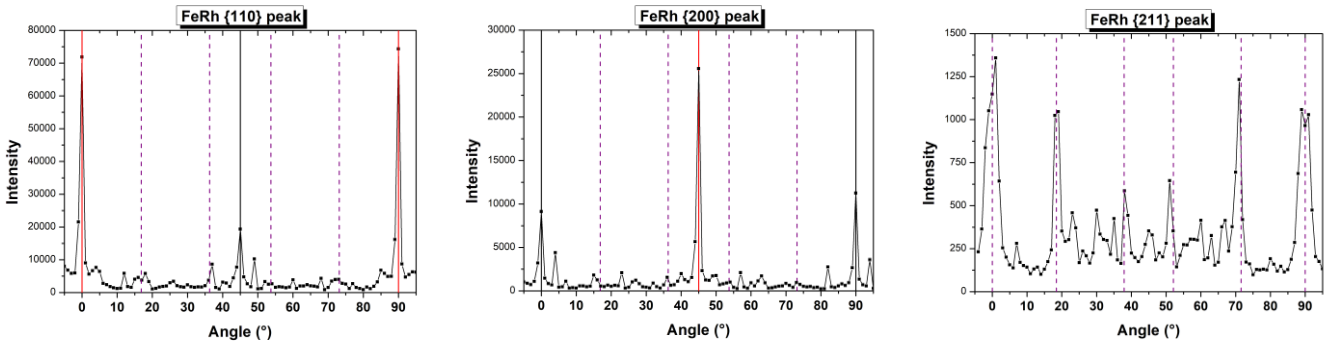

Fig. 9: angular dependence of the intensity of different FeRh peaks. The favorable orientations corresponding to the two "cube-on-cube" epitaxy relationships are indicated with red and black lines (red=usual epitaxy, major contribution) while purple dotted lines correspond to coincidence between $\{211\}_{FeRh}$ and $\{310\}_{STO}$ (multiple possibilities taking into account the symmetries) for particles on a {110} facet. Note that the {211} ring cannot correspond to particles lying on a {001} facet.

A few out-of-plane measurements (L-scans) have also been performed (see Fig. 10), in order to study the orientation of FeRh crystals on the surface. The obtained data are consistent with the analysis described above with the coexistence of particles lying on {001} facets (major contribution) and some particles lying on {110} facets (responsible for the {211} ring).

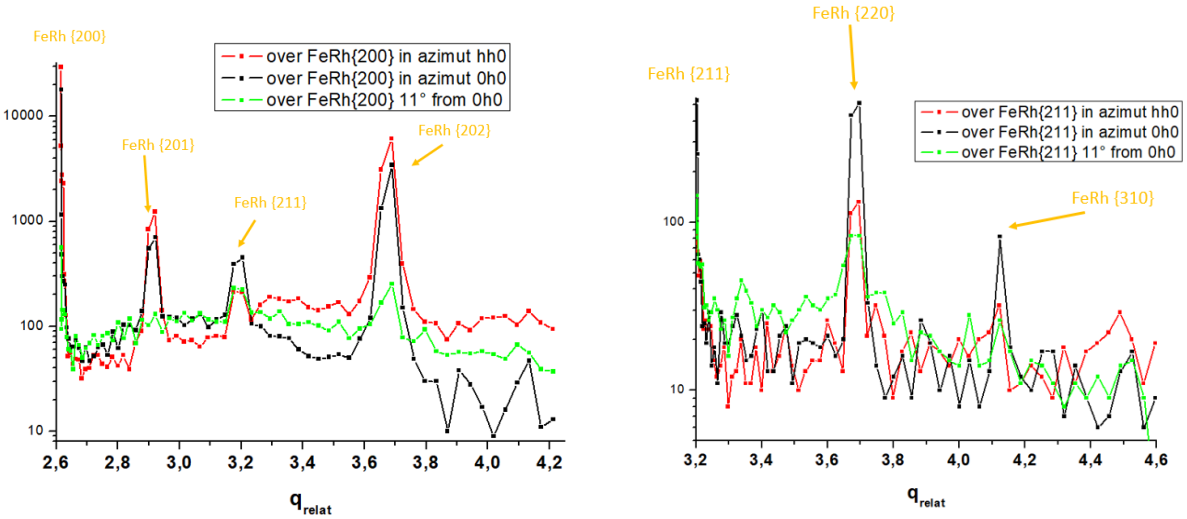

Fig. 10: L-scans (perpendicular to the surface), after annealing, over different locations in the surface plane.

Conclusion

Thanks to the allocated beam time, we have been able to successfully observe in situ the transition from A1 to B2 phase, as well as the appearance of a coherent orientation of FeRh nanoparticles on the surface of both BTO thin film and STO single crystal. Remarkably, epitaxy relationships specific to this system have been put into evidence: the two "cube-on-cube" epitaxy relationships (particles on a {001} facet) for BTO thin film and STO, and an original favorable coincidence between $\{211\}_{FeRh}$ and $\{310\}_{STO}$ (particles on a {110} facet). A significant coalescence between FeRh particles seems to occur for samples on perovskite surfaces annealed up to ~700°C. Nevertheless, it should be noted that the typical diameter remains under 20 nm, and that this estimated size may not reflect the entire particle size distribution on the surface: the contribution from larger particles can indeed "artificially" dominate the signal, or the particles adopting favorable orientations on the surface may be the largest ones in the assembly… Anyway, additional investigation on this interesting system are needed.